A Cognitive Spatial Learning Control System for 3-Dimensional Random Arrays

Jeffrey S. Jensen and Gregory H. Huff, Department of Electrical and Computer Engineering, Texas A&M University, College Station, Texas, USA. (jeffsanwa@tamu.edu)

Key Points

Random geometries are prevalent in mobile intelligent system coordination

Node position in random volumetric arrays is essential to array control

Image processing techniques improve accuracy for random array control

Abstract

This work proposes the combined use of spatial recognition techniques and infrared depth-of-field sensing in a phased array control system for morphing clusters of randomly distributed antennas. The system is designed to uniquely identify array elements (or platforms) and track the motion-dynamic spatial distribution to provide feedback and control information for phase shifting and beamforming. The specific focus of this work is to examine the core performance of the phased array control system. This begins with the use of spatial recognition algorithms in a discovery phase to establish element identities and analyze their locations in the optical field of view. This process informs the accompanying depth-of-field sensor so it can evaluate the spatial distribution of elements and enable the tracking of element locations in time. This information is relayed to a distributed array controller that identifies the bounding manifold of the array (curvilinear, spheroidal, etc.), and calculates phases for the elements to achieve the desired beam steering operation. The system also includes a user interface for a mobile device (smartphone, tablet, etc.) which can be used to control the phased array and link geolocation information for autonomous tracking modes. A system operating at 2.4 GHz has been constructed using low-cost off-the-shelf components, as well as custom-designed element platforms so the performance of the system can be observed experimentally. Results for element identification and spatial distribution are included to benchmark the accuracy of the aforementioned system.

Index Terms – Signal processing (0674), Space and satellite communication (6979), Instruments and techniques (6994)

1. Introduction

Low-cost vision systems and open-source computer vision libraries have emerged as viable tools for the development of spatial awareness techniques for intelligent and autonomous systems. The specific use and advantage of these tools derive from tightly coupled color and depth images that link visual environmental properties with a respective physical location. These tools have been extensively developed and successfully utilized for a variety of applications [Kanezaki et. al., 2011; Nakamura, 2011; Clark et. al., 2014] related to object tracking, terrain mapping, and collaborative task management. These spatial recognition techniques have also been used with autonomous vehicles, unmanned air vehicles (UAVs), and micro air vehicles (MAVs) to improve their autonomous control and coordinate complex movements in clusters or swarms [Moshtagh et. al., 2009].

The combined use of color and depth of field information in these application spaces has enabled the analysis of clustered objects in a single frame of reference. It also reduces the computational complexity and enables further research of swarms and clusters in applications of mobile ad-hoc networks as in [Ochiai et. al., 2005; Warty et. al., 2013] and autonomous vehicle collaboration. Distributed sensor networks leverage local node processing power for data acquisition, temporary storage, and conditional pre-processing. These individual pieces of information can be holistically analyzed to reveal profitable system-wide analytics, statistics, and other metrics that

have widespread applications. These networks have derived increased performance and information capabilities when the spatial distribution of nodes in the cluster was dynamic. Networked swarms of UAVs are one such platform that has been researched to perform mobile sensing tasks and to fly collectively in various formations as in [Dac-Tu Ho, 2013]. This type of collaboration has allowed groups of UAVs to accomplish tasks together that a single UAV could not accomplish alone. Coordination in both static and dynamic applications is typically conducted through wireless data streams that must handle dynamic adjustments to the wireless channels. Increasing node count results in a commensurate complex electromagnetic environment. This leads to several wireless challenges including channel interference, local synchronization problems, and additional hardware communication issues.

Electromagnetic design and spatial control therefore play an important role in defining wireless performance of a clustered network and its communication capabilities. The dynamic cluster is of particular interest because of the electromagnetic implications that arise with changing position and configuration of communications hardware. A single UAV antenna and radio are useful for peer-to-peer communications and for direct communication with a base station in close proximity. It can be shown however that enriched electromagnetic and communication ability can be derived from coordinated use of each node's antenna and radio into a phased array configuration as in [Ochiai et. al., 2005]. Immediate benefits of coordinated radios and antennas include increased gain, directivity, and communication distance. Phased array configurations in both static and dynamic cases contain elements that may be aperiodic (random) with respect to wavelength causing non-deterministic array behavior [Buchanan and Huff, 2014]. Network-centric control of these random geometries presents several complex problems including spatial

awareness, local oscillator synchronization, and collective signal phasing. Wireless local oscillator synchronization will not be considered in this work but remains an important area of research for random arrays and dynamic clusters [Baldoni et. al., 2010; Chen et. al., 2010]

The scope of this work focuses on a novel system that detects spatial configurations and provides element phasing of random arrays within dynamic-positioning clustered frameworks. Previous work on random arrays in recent years is presented with an emphasis on element positioning and phasing control complexities. An autonomous phased-array control system is presented as a useful and scalable platform for phasing control of random arrays. Inclusion of infrared spatial discovery techniques from a Microsoft Kinect camera using computer vision algorithms is then presented as an extension of the phased array control system. An intelligent antenna design modeling a UAV has been designed and fabricated for system tests. A spatial detection experiment has been conducted and the results provide the capabilities of the proposed system.

2. Previous Work

Random arrays have been studied extensively in the past few decades from theoretical and mathematical standpoints [Harrington, 1961; Lo, 1964]. New application demands utilizing beam steering, side lobe tapering, and geometrical optimization techniques have focused efforts on fabrication, control, and physical performance of random arrays [Buchanan et. al., 2014]. The resulting systematic control of random arrays for these applications has been complex due to control requirements that demand continuous observations, calculations, and reactions to preserve or achieve desired radiation behavior. Element position directly impacts the array factor that is combined with the element pattern to generate radiation behavior. The uniformly excited

array factor encapsulates both element position and a desired beam scanning angle (θ,φ) shown in (1).

$$AF(\theta,\phi) = I_0 \sum_{m=1}^{M} e^{j(m-1)(kd_x \sin(\theta)\cos(\phi)+\beta_x)} \sum_{n=1}^{N} e^{j(n-1)(kd_y \sin(\theta)\sin(\phi)+\beta_y)} \sum_{p=1}^{P} e^{j(p-1)(kd_z \cos(\theta)+\beta_z)} \quad (1)$$

The wave number *k* and relative displacement *d* contribute with sine and cosine angular factors to generate progressive phase shifts for each element in Euclidean space given by (2), (3), and (4).

$$\beta_x = -kd_x \sin(\theta)\cos(\phi) \quad (2)$$

$$\beta_y = -kd_y \sin(\theta)\sin(\phi) \quad (3)$$

$$\beta_z = -kd_z \cos(\theta) \quad (4)$$

These progressive phase shifts dictate the behavior of beam-steering, sum-difference, and other radiation patterns. Progressive phase shift control was examined in previous work from [Buchanan et. al., 2014] through a fabricated a microstrip patch array that used phasing information in an array controller to achieve beam steering and sum-difference radiation patterns.

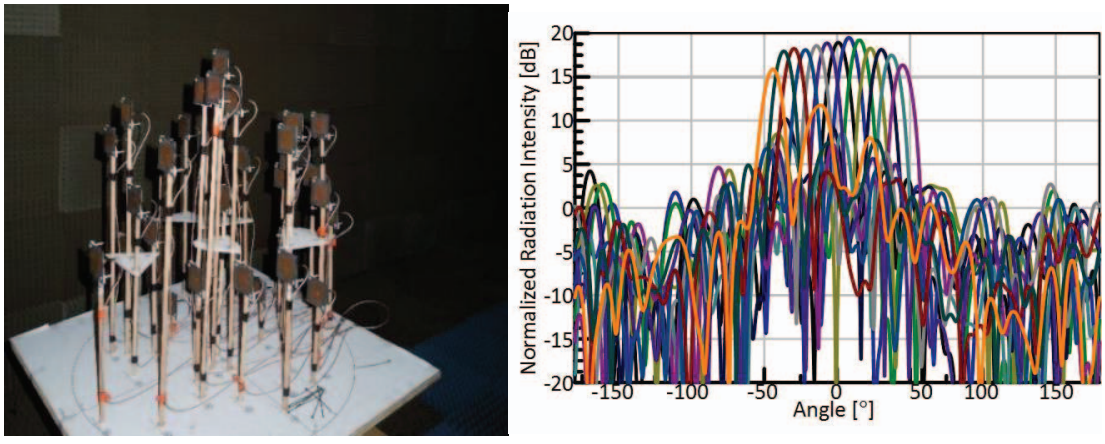

Figure 1. (Left) Microstrip patch volumetric random array (Right) Measured radiation pattern from array

The radiation pattern in Figure 1 displays a successful 7.5 degree incremental beam-steering radiation scan from -45 to + 45 degree of a 32 element volumetric array. This work utilized a smartphone enabled phased array controller that simultaneously controlled 32 individual element phases. The authors note that the controller could not generate phases without prior knowledge of the element position and required individual Euclidean manual measurements. These coordinates were either hard-coded or sent from the smartphone into the controller to produce accurate phase results. This meticulous error-prone process arises in tightly coupled distributions such as in Figure 1. It is therefore advantageous to expand the system to eliminate the source of human error and provide a closed loop spatial detection technique.

3. System Architecture

The automated phased array system in [Buchanan et. al., 2014] has two primary control components. A smartphone provides the first component. It gathers geolocation information from on-board GPS sensors and externally-determined element locations in 3-dimensional space. Localization data and element positions provide information for phase delay calculations and angular steering functions. The smartphone wirelessly transmits this post-processed data to an embedded control system. This modular controller converts scanning angles to individual element phases that are calculated according to (2), (3) and (4). These phases are converted to a voltage through a 16-bit digital to analog (DAC) and applied to the phase shifter through a mapping process that transforms the 0V-12V output to a corresponding phase shift spanning 0° to 450°.

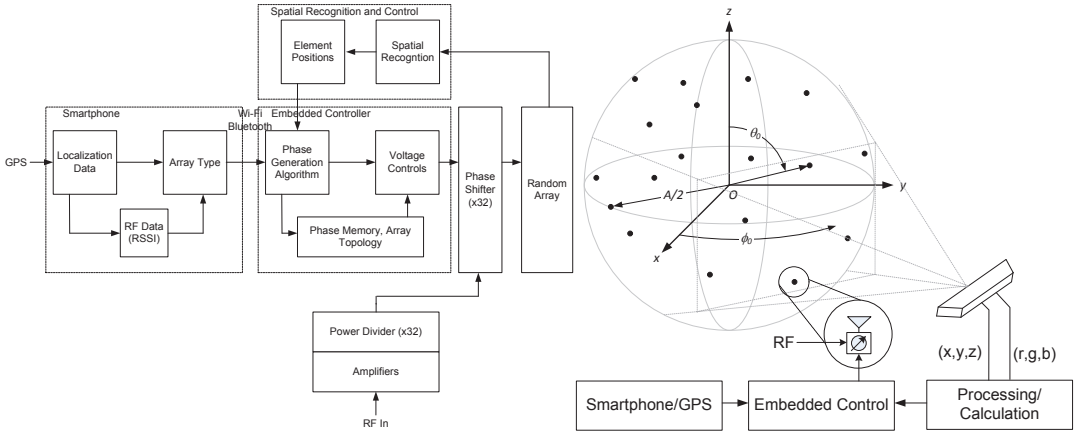

Figure 2. (Left) Random array system control diagram (Right) High level system diagram

The radio frequency (RF) signal in the experiment was single sourced and progressed through a network of amplifiers and power dividers before reaching individual phase shifters. This varies from the current problem as spatially displaced individual elements would require independent synchronization of RF paths or local oscillator synchronization seen in [Baldoni et. al., 2010; Chen et. al., 2010]. This realization is not included in this work but can be adapted to the proposed system in future work. The proposed novel architecture leverages the existing platform's ability to calculate element phases and wireless GPS localization capability through the smartphone. The fundamental addition is a spatial recognition and tracking component as seen in Figure 2. The spatial recognition and detection component presented in this work provide element position data to generate phasing information for the random array. Discovered elements are localized within the cluster, and can be cached to memory or communicated to the control system. Cached elements are tracked for any positional changes during array control operations and any positional change can be communicated to the controller for phase adjustment. The previous tests results from [Buchanan et. al., 2014] include an additional intrinsic delay of the RF

path that had to be measured for each element. This phase error must also be included in the individual element phasing calculation as shown in (5).

$$\beta_{tot} = \beta_x + \beta_y + \beta_z + \delta_{path} \tag{5}$$

This resultant phase delay for each individual element is a combination of element position and the intrinsic RF path delay due to the amplifier, power divider, phase shifter, and cable connections.

4. System Materials

The implementation of the computer vision assisted phased array architecture requires hardware for spatial detection and recognition. The Microsoft Kinect was originally intended as a peripheral controller for Xbox 360 as it provides 640x480 pixel color and depth (denoted RGBD) data streams for computer-human interaction at a sampling rate of 30 Hz [Noonan et. al., 2011]. The camera was originally developed by PrimeSense™ and uses a proprietary pseudo-random infrared detection technique for spatial displacement measurement. Infrared light scatters from the surface of an object to be projected into the receiving plane of the Kinect camera. Real world x, y, and z coordinates can be calculated and calibrated using internal parameters from the camera [Noonan et. al., 2011]. The final combined camera data stream provides a 640x480 matrix of data which contains a red, green, and blue (RGB) 8-bit color code and a real world (x,y,z) coordinate for that specific pixel. This enables simplified environment awareness and object detection from both color and depth data streams. Color filtering is of particular interest due to minimally complex threshold filtration algorithms and a natural occurrence in both color and depth images. Color filtering is also agnostic of the image generation source and can be

adapted to platforms such as Microsoft Kinect, LIDAR cameras, and other high resolution imaging hardware [Lili and Barth, 2011].

4.1 Antenna Design

Using the Microsoft Kinect's color and data information for spatial detection requires uniquely identifiable colored targets. Realistic targets for this system require a functional antenna design and a realization of common hardware frameworks utilized in autonomous vehicle swarms. The proposed platform combines these two requirements to produce a highly configurable and extendable embedded antenna platform to emulate autonomous swarm systems.

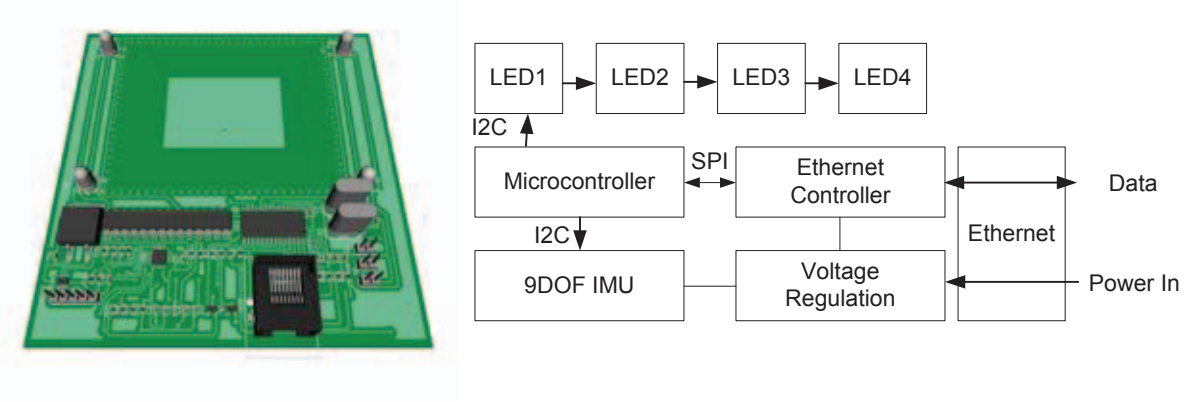

Figure 3. (Left) 3-D antenna module design (Right) Block diagram for antenna module

A patch antenna on FR4 substrate ($\varepsilon_r = 4.4$) was designed for an operating frequency of 2.45 GHz to align with results produced in [Buchanan et. al., 2014]. The substrate is shared with an embedded microcontroller, Ethernet controller featuring power over Ethernet (POE), a nine degree-of-freedom (9DOF) inertial measurement unit (IMU), and four (4) RGB light emitting diodes (LEDs). A separate ground plane and through-hole via fence have been included in this

design to electrically isolate the RF system and embedded circuits. Color configuration of the LEDs is communicated from a central control station through Ethernet to the microcontroller. The LEDs have also been placed in a rectangular distribution to enable easier discovery by the spatial recognition system. The microcontroller is capable of interrogating the IMU for rotation and temperature information to be communicated back to the central control system for further processing and calculation. Additional control pins of the microcontroller have been left unconnected for further adaptations and designs such as quad rotors, reconfigurable antennas, or other applications.

5. Software System Design

The software architecture is comprised of four separate stages: calibration, acquisition, calculation, and reaction. The first stage requests system calibration of the visual device to minimize measurement error in high noise environments. Subsequent spatial calibration of the Kinect can be run to remedy erroneous results or to reset error bounds used in position detection and estimation [Noonan et. al., 2011].

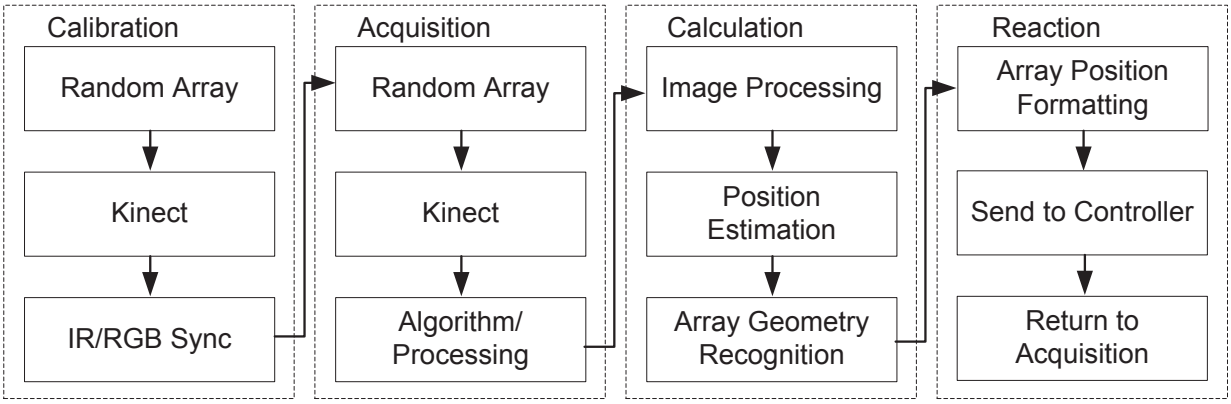

Figure 4. Block diagram for system software architecture

The acquisition stage defines an interface to gather visual information from the visual source to be processed in the object detection algorithm contained within the calculation stage. Multi-threaded calculation processes also spawn to extract information from color and depth images to be analyzed in the calculation stage. Threading is needed due to heavy demand of computing resources used during image processing techniques. The calculation stage processes image data acquired by the acquisition stage using image filtering techniques such as color thresholding, dilation, and erosion. The position detection and estimation calculation is dependent on pattern recognition in the RGB image in this system. Successful recognition yields a specific point of interest (POI) to be analyzed from the depth image. Cross correlation of the POI in the depth image finds the estimated location from the depth image. The position in Euclidean space is saved in storage for processing in the reaction stage. This stage is comprised of a control and data layer which communicates with the existing controller to calculate phases for each array element.

5.1 Image Processing

Several fields in computer science including robotics, artificial intelligence, and object recognition utilize complex image processing techniques to enable intelligent systems to recognize objects in their environment [Clark et. al., 2014; Kanezaki et. al., 2011; Nakamura, 2011]. Commonly used techniques in object recognition rely heavily on color transforms. These transforms provide a distinct advantage to computers and systems by mapping color information into different vector spaces and coordinate systems to simplify calculation and pattern matching.

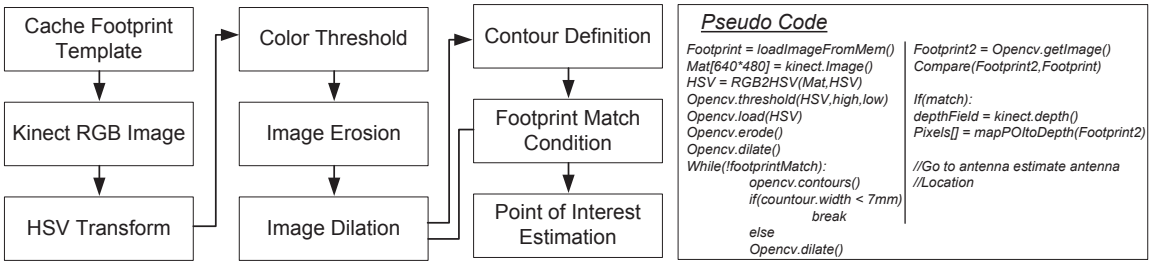

Figure 5. (Left) Image processing progression steps (Right) Pseudo code for detection algorithm

Pattern matching is essential to object discovery and tracking. The proposed image processing algorithm in Figure 5 caches a desired footprint or pattern that is continuously analyzed in each RGB frame by the system. The proposed pattern footprint contains two large white areas housing 4 small areas that represent the 4 LED locations on the modular antenna shown in Figure 6. The algorithm caches an RGB image and performs a common HSV color space color transformation. The HSV color space is a cylindrical transform that represents the luminance of colors that are observed in an image by incorporating the value (V) or brightness of the color. This algorithm uses color thresholds that have been empirically discovered due to varying brightness of LEDs on the antenna module. Unique color configurations for each antenna module require unique color thresholds bounds. Small threshold bounds permit greater use of colors of the same spectrum and reduce ambient color noise in the binary image. The produced binary image may still contain undesired noise from the surrounding environment that can be eliminated by eroding the image. A loop then continues to dilate the image until the black spaces representing the pixels have a matched depth location of 7mm or less. An average footprint with standard deviation is shown in Figure 6. This measurement is within 1mm of the actual physical LED size of 5 mm.

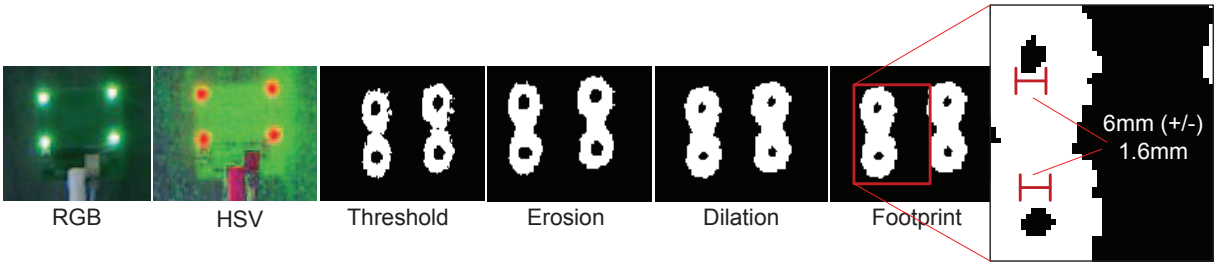

Figure 6. Image progression for detection algorithm

The final image should emulate or directly match the cached pattern to produce a point of interest. Points of interest are also cached in small arrays for time averaging. Averaging the points of interest filters any additional noise and erroneous outliers.

5.2 Position Estimation

The filtration process described in 5.1 produces points of interest that correspond to the LEDs in the four corners of the patch antenna. Each point of interest is defined with an additional real world x, y, and z coordinate from the Kinect's depth stream. These coordinates are used to calculate the antenna's position in Euclidean space.

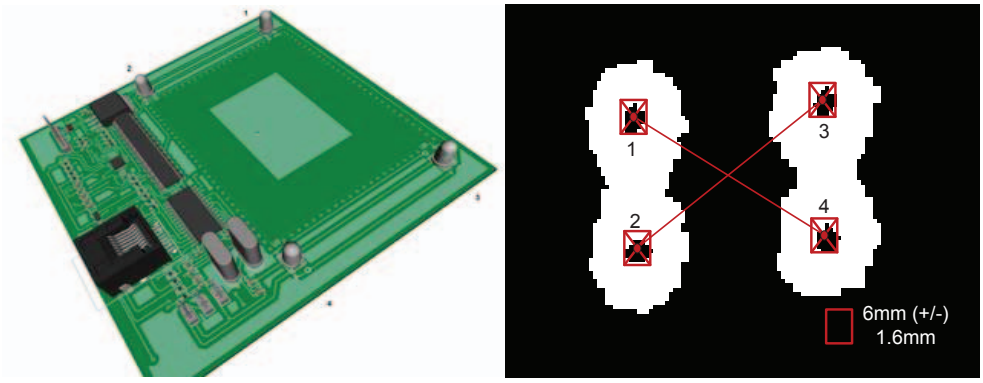

Figure 7. (Left) Fabricated antenna module with numbered pixels (Right) Footprint matching with numbered pixels

The antenna's position is calculated by averaging the diagonal vectors from pixels 1 to 4, and 2 to 3 as shown in Figure 7. This process is explicitly noted in (6) and (7).

$$\vec{L}_m = \{x, y, z\} \mid m = center, 1, 2, 3, 4 \tag{6}$$

$$\vec{L}_{center} = ((\vec{L}_1 + \vec{L}_4)/2 + (\vec{L}_2 + \vec{L}_3)/2)/2 \tag{7}$$

The average finds the center point of the module which is stored in memory to be compared to other modules in the random array. A center point and footprint pixel location provide additional measurement mechanisms to verify the precision and accuracy of the resultant location shown in (7). These additional references provide physical dimensions that correspond to known dimensions of the antenna and when compared yield an estimation error that is used to further average the result shown in (7).

6. System Fabrication and Testing

A system based on design criteria and proposals from sections 4 and 5 was developed. Three antenna modules were fabricated and tested for experimental use as shown in Figure 8.

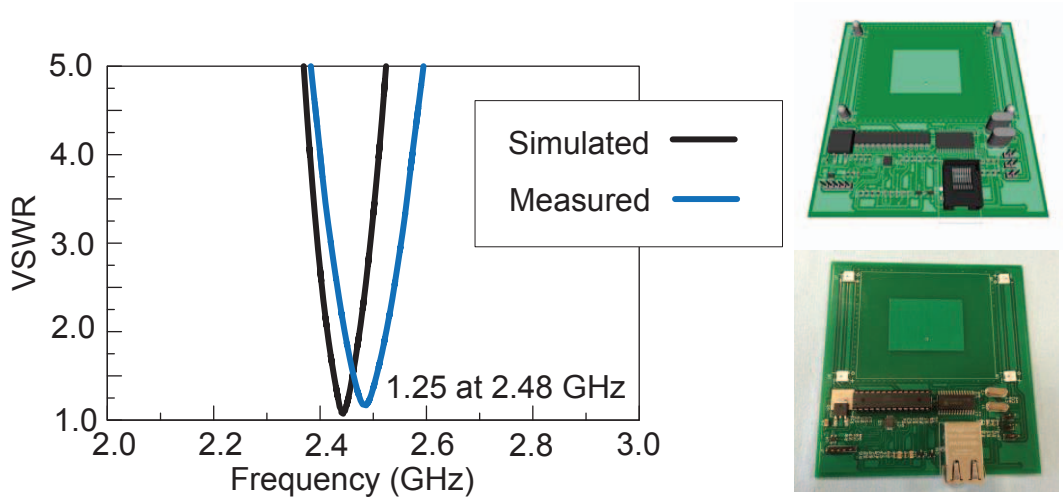

Figure 8. (Left) VSWR of simulated and fabricated antenna modules (Upper Right) Simulated antenna (Lower Right) Fabricated antenna

Measured antenna results compared to simulation show a shift of approximately 20 MHz in frequency. The impedance result shows a disparity outside of the resonant frequency due to an initial offset that was not subtracted in the calibration. The antenna modules used a single cable for network connection and power supply during the experiment. The goal of the experiment was to determine the accuracy of the system with the Kinect as a visual-spatial acquisition tool for random array geometries. Accuracy in these experiments is defined as the comparison of the Kinect measured positions in their relation to a resultant phase error according to (2), (3) and (4) using the measurement error. The Kinect was placed at varying distances from the closest element in the array to gain insight about optimal viewing distances of the camera to most accurately measure element position.

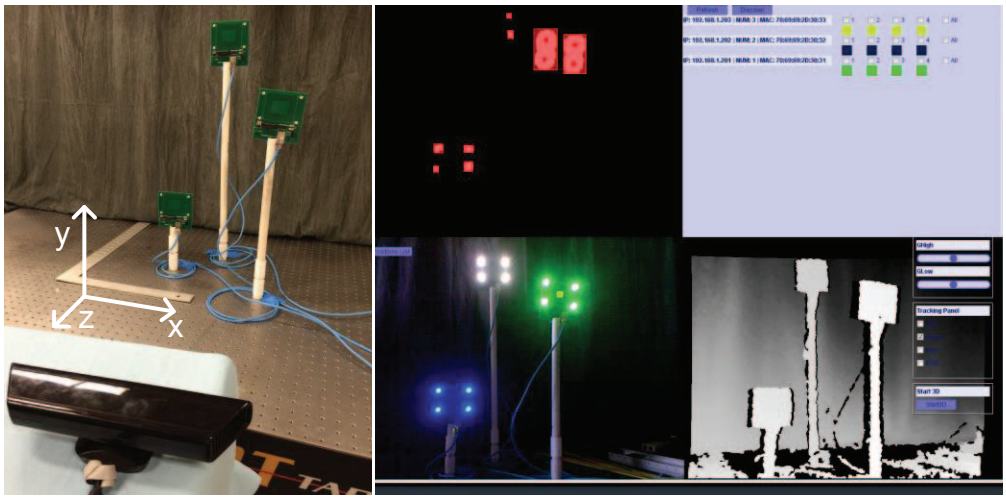

Figure 9. (Left) Three antenna experimental setup (Right) Screen shot of software controller and Kinect tracking green antenna module

The antennas were placed in a dark room to eliminate ambient light noise and were attached to three height-varying mounts on a measurement table. The Kinect camera connected to a computer which ran the system control software that performed all image processing and communication with the pre-existing phasing controller.

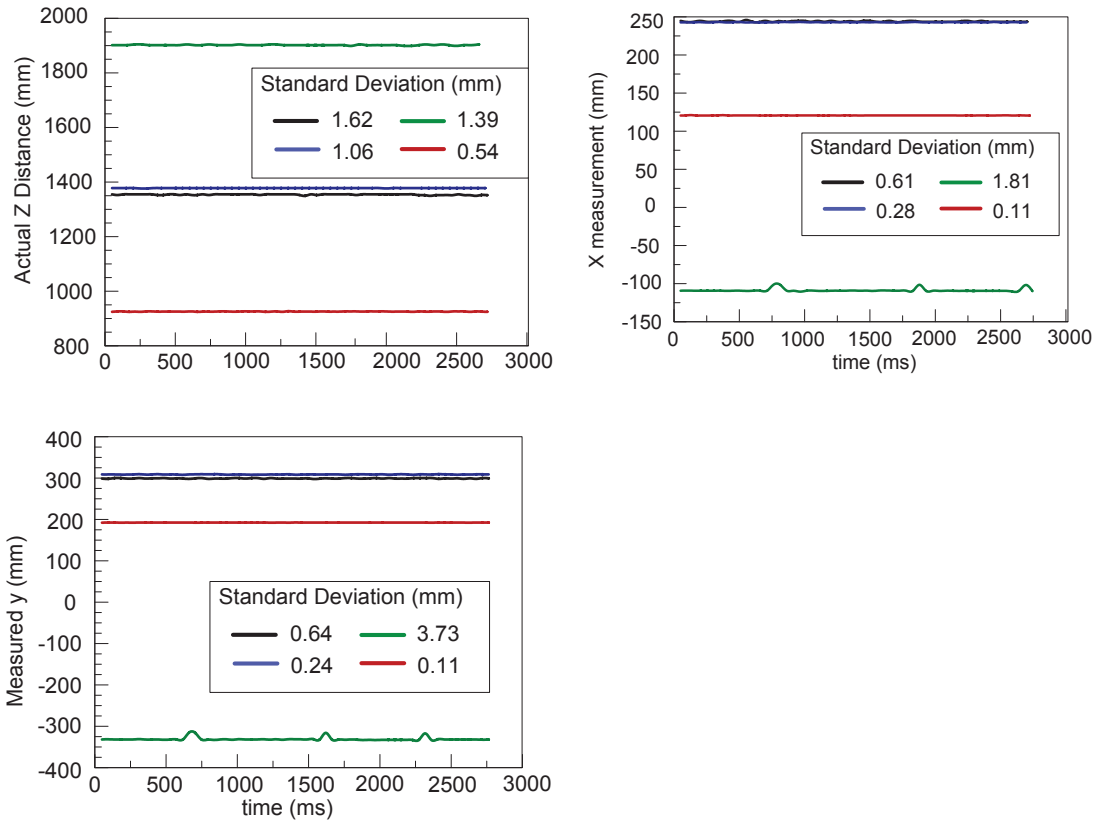

Figure 10. Standard deviation measurements for real world x, y, and z coordinates

The graphs in Figure 10 show (x,y,z) coordinates for the closest antenna to the Kinect for four varied distances. Standard deviation increased as the Kinect moved away from the array to accommodate larger aperture size but had sub-millimeter drift in close proximity ($z < 1m$). This indicated that the image processing algorithm could successfully detect and track an element location with minimal change during time. A tradeoff is that as an aperture size increases the Kinect will be forced to move farther away increasing the potential for measurement error. Positions from the Kinect were then compared with hand measurements. Kinect spatial detection error in millimeters averaged between 4 – 8 mm with a worst case estimation error of 14 mm in the y axis at distance of 925 mm from the closest antenna. The measurement error and error

range present the possibility of using this spatial recognition technique as a 4-bit or 3-bit phase shifter.

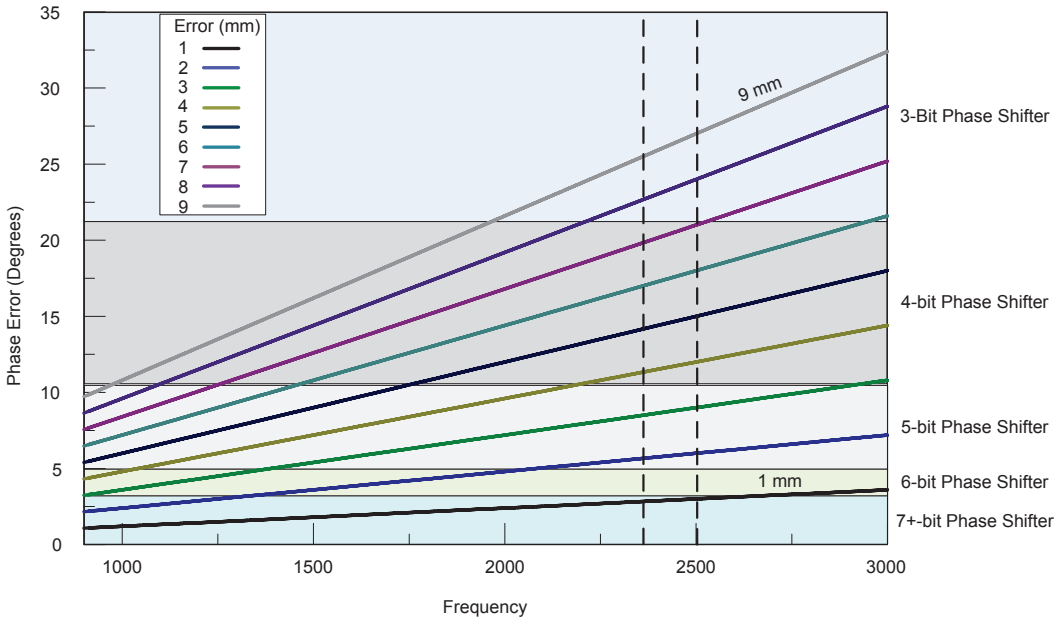

Figure 11. Relation between frequency, phase error, measurement error, and n-bit phase shifters

This result is important because it provides a unique metric for evaluating the system at the design frequency in terms of potential phase error. The measurement error produces a phasing error that additively contributes to the total phase delay the antenna element experiences. It is therefore important to reference an n-bit phase shifter for the respective frequency and measurement error to determine beam-steering capabilities of the system. This metric additionally reemphasizes the importance of minimizing measurement error with higher resolution cameras and better spatial detection techniques such as those used with LIDAR.

6.1 Error Tolerance in Random Arrays

The estimation error of the Kinect and array system allows the phase shifter controller to operate at 4-bit phase shifter accuracy. This calculation was derived from equations (2) - (4) where the resultant phase error at a frequency of 2.4 GHz for 1mm error in measurement is approximately 2.88 degrees. A simulation using microstrip patches from [Buchanan et. al., 2014] was performed to view the potential effects of these phase errors in the random array system. The antenna modules presented have not been measured but a comparison in element pattern is presented in Figure 12.

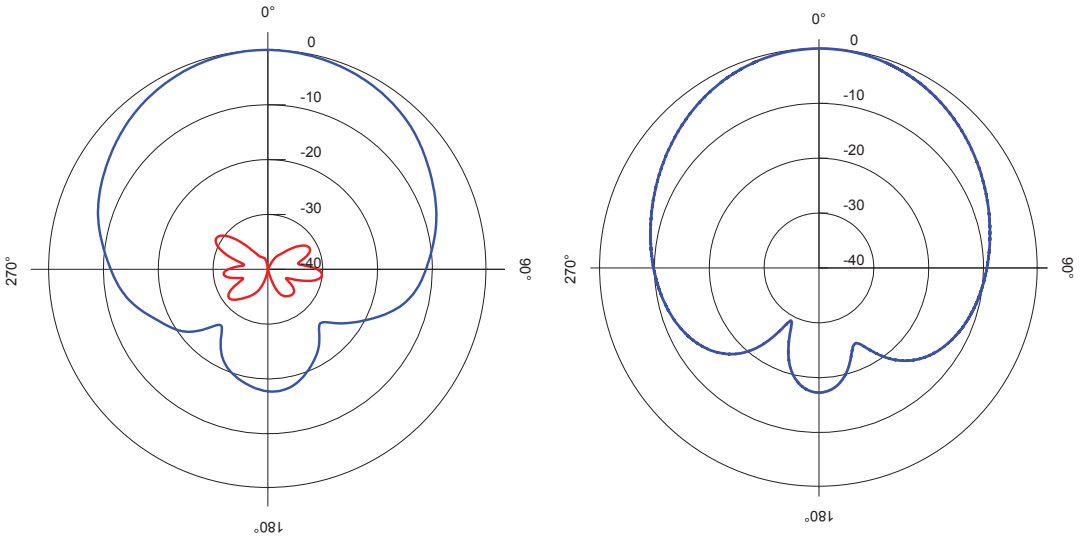

Figure 12.(Left) Microstrip patch from [Buchanan et. al., 2014] (Right) Antenna module radiation pattern for $\theta = 90^{o}$, $\varphi = 0^{o}$

The comparison of the two radiation patterns better predicts simulated models of the antenna modules in a fabricated physical array. After the element pattern was simulated, a 3-element array resembling the experiment was simulated to observe how the phase error impacts the radiation behavior of the array. Elements were simulated with the correct phase shift and then a randomized 4-bit phase shift error of (+/-) 22.5 degrees.

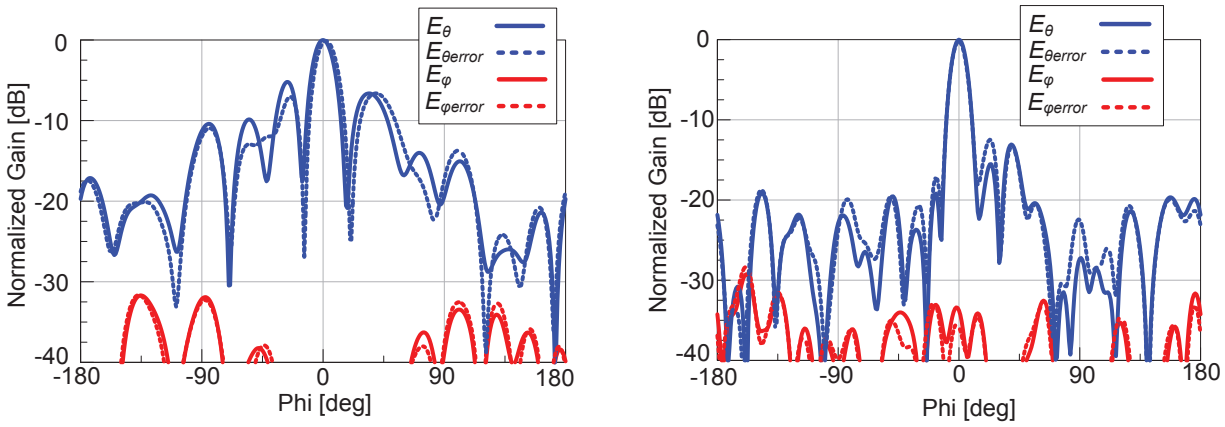

Figure 13. (Left) 3 Element simulated normalized gain radiation pattern (Right) 32 Element simulated normalized gain radiation pattern, both in plane: $\theta = 90^o$, $\varphi = 0^o$

The three element array is affected by the phase error output as it shifts the main beam off axis approximately 3 degrees. Sidelobe behavior is also effected as nulls are increased and an angular shift of maximum 6 degrees also occurs. The simulation was expanded to a 32 element array shown in Figure 13 to emulate the experiments performed in [Buchanan et. al., 2014] with a similar randomized phase error performed in the 3 element array. The main beam of the 32 element array shifts less than 1 degree and the first sidelobe of the main beam increases by 3 dB.

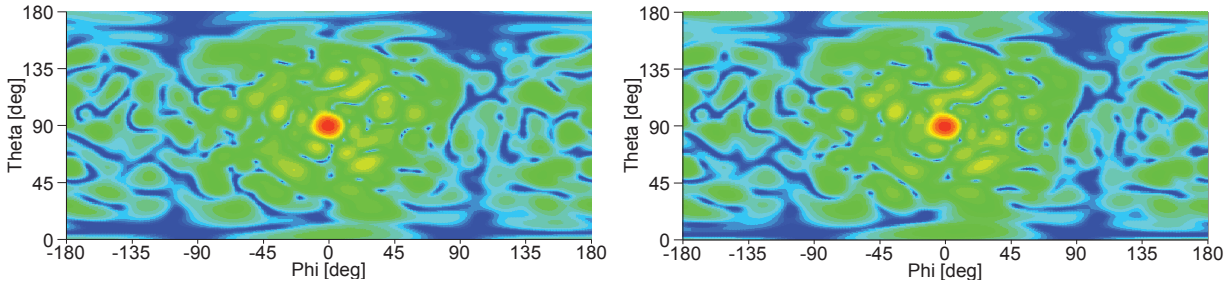

Figure 14. Normalized gain radiation pattern for (Left) exact phase shift 32 element array (Right) randomized 4-bit phase error 32 element array

Figure 14 shows a holistic and comprehensive view of the exact and randomized 4-bit error phase shifting radiation patterns displaying less than 1 degree of angular shift of the main beam. The sidelobe behavior of the 4-bit randomized array shows unsymmetrical shifts and increased gains of the closest sidelobe that is additionally seen in Figure 13 due to the randomized 4-bit error.

7. Conclusion and Future Work

A spatial recognition and ranging system for the detection and tracking of element positions for random arrays has been presented. A system architecture using the Microsoft Kinect as a spatial discovery tool was designed and realized. Configurable antenna modules resembling UAVs have been designed and presented as realistic targets for a spatial recognition and tracking system. An abstracted image processing software architecture presented accurate and precise capabilities for tracking the designed antenna modules. Fabrication of the antenna modules and subsequent experiments yielded results that the phased array control system, using spatial recognition techniques, operates in comparison with a 4-bit phase shifter. Overall, the complex dichotomy between the spatial recognition system and respective targets has been simplified through hardware and system design. This system was designed for several RF hardware platforms and can be abstracted in software design to accept various forms of inputs and variants to the data from other imaging sources. Future work includes testing various random array geometries of 16 and 32 element random arrays on the fabricated platform shown in Figure 15 whose ‘arms’ or hoisting elements can be moved and fixed into random/various geometries.

Figure 15. (Left) 16 element random array test apparatus (Right) Side view of test apparatus

Overall, position estimation can be improved with further investigation into the image processing techniques, a higher resolution camera, and real-time calibration techniques; however, the random array control system, using the Kinect for spatial recognition techniques, provides a potential platform to perform closed loop position estimation control in volumetric aperiodic arrays.

8. Acknowledgments

This material is based upon work supported by, or in part by, the US Army Research Laboratory and the US Army Research Office under agreement number W911NF-09-1-0429

9. References

Baldoni, R.; Corsaro, A.; Querzoni, L.; Scipioni, S.; Piergiovanni, S.T., "Coupling-Based Internal Clock Synchronization for Large-Scale Dynamic Distributed Systems," *Parallel and Distributed Systems, IEEE Transactions on* , vol.21, no.5, pp.607,619, May 2010
doi: 10.1109/TPDS.2009.111

Buchanan, K.; Huff, G. H., "A Stochastic Mathematical Framework for the Analysis of Spherically-Bound Random Arrays," *Antennas and Propagation, IEEE Transactions on* , vol.62, no.6, pp.3002,3011, June 2014
doi: 10.1109/TAP.2014.2313142

Buchannan, K., Jensen, J., and Huff, G. H., "An Android-Controlled Direction of Arrival System using Polarization-Reconfigurable Antennas," *in proc. Antenna Applicat. Symp.*, Monticello, IL, Sept. 2014, pp. 101-12.

Chen, Y.; Dickens, J.; Holt, S.; Reale, D.; Mankowski, J.; Kristiansen, M., "Synchronization of phased array pulsed ring-down sources using a GPS based timing system," *Power Modulator and High Voltage Conference (IPMHVC), 2010 IEEE International* , vol., no., pp.624,627, 23-27 May 2010
doi: 10.1109/IPMHVC.2010.5958436

Clark, M.; Feldpausch, D.; Tewolde, G. S., "Microsoft kinect sensor for real-time color tracking robot", *Electro/Information Technology (EIT), 2014 IEEE International Conference on,* On page(s): 416 – 421

Dac-Tu H.; Grotli, E.I.; Sujit, P.B.; Johansen, T.A.; Borges de Sousa, J., "Performance evaluation of cooperative relay and Particle Swarm Optimization path planning for UAV and wireless sensor network," *Globecom Workshops (GC Wkshps), 2013 IEEE* , vol., no., pp.1403,1408, 9-13 Dec. 2013
doi: 10.1109/GLOCOMW.2013.6825191

Harrington, R.F., "Sidelobe reduction by nonuniform element spacing," *Antennas and Propagation, IRE Transactions on* , vol.9, no.2, pp.187,192, March 1961
doi: 10.1109/TAP.1961.1144961

Ishimaru, A., "Theory of unequally-spaced arrays," *Antennas and Propagation, IRE Transactions on* , vol.10, no.6, pp.691,702, November 1962
doi: 10.1109/TAP.1962.1137952

Jurado, F.; Palacios, G.; Flores, F., "Vision-Based Trajectory Tracking on the 3D Virtual Space for a Quadrotor", *Electronics, Robotics and Automotive Mechanics Conference (CERMA), 2012 IEEE Ninth,* On page(s): 31 – 36

Kanezaki, A.; Harada, T.; Kuniyoshi, Y., "Scale and rotation invariant color features for weakly-supervised object Learning in 3D space," *Computer Vision Workshops (ICCV Workshops), 2011*

IEEE International Conference on , vol., no., pp.617,624, 6-13 Nov. 2011
doi: 10.1109/ICCVW.2011.6130300

Lili H.; Barth, M., "Tightly-coupled LIDAR and computer vision integration for vehicle detection," *Intelligent Vehicles Symposium, 2009 IEEE* , vol., no., pp.604,609, 3-5 June 2009
doi: 10.1109/IVS.2009.5164346

Lo, Y.T., "A mathematical theory of antenna arrays with randomly spaced elements," *Antennas and Propagation, IEEE Transactions on* , vol.12, no.3, pp.257,268, May 1964
doi: 10.1109/TAP.1964.1138220

Moshtagh, N.; Michael, N.; Jadbabaie, A.; Daniilidis, K., "Vision-Based, Distributed Control Laws for Motion Coordination of Nonholonomic Robots," *Robotics, IEEE Transactions on* , vol.25, no.4, pp.851,860, Aug. 2009
doi: 10.1109/TRO.2009.2022439

Nakamura, T., "Real-time 3-D object tracking using Kinect sensor," *Robotics and Biomimetics (ROBIO), 2011 IEEE International Conference on* , vol., no., pp.784,788, 7-11 Dec. 2011
doi: 10.1109/ROBIO.2011.6181382

Noonan, P.J.; Cootes, T.F.; Hallett, W.A.; Hinz, R., "The design and initial calibration of an optical tracking system using the Microsoft Kinect," *Nuclear Science Symposium and Medical Imaging Conference (NSS/MIC), 2011 IEEE* , vol., no., pp.3614,3617, 23-29 Oct. 2011
doi: 10.1109/NSSMIC.2011.6153680

Ochiai, H; Mitran, P.; Poor, H.V.; Tarokh, V., "Collaborative beamforming for distributed wireless ad hoc sensor networks," *Signal Processing, IEEE Transactions on* , vol.53, no.11, pp.4110,4124, Nov. 2005
doi: 10.1109/TSP.2005.857028

Waddell, M.; Villasuso, J.; ChavezGuevera, D.; Jong-Hoon K., "Standardized linearization and vectorization algorithm for arm motion control of a humanoid telepresence robot", *Robotics (ISR), 2013 44th International Symposium on,* On page(s): 1 - 6

Warty, C.; Yu, R. W.; ElMahgoub, K.; Spinsante, S., "MUSIC algorithm DoA estimation for cooperative node location in mobile ad hoc networks," *Aerospace Conference, 2013 IEEE* , vol., no., pp.1,8, 2-9 March 2013
doi: 10.1109/AERO.2013.6497422

Yimin, Z.; Guolai, J.; Guoqing, X.; Xinyu, W.; Krundel, L., "Kinect depth image based door detection for autonomous indoor navigation," *Robot and Human Interactive Communication, 2014 RO-MAN: The 23rd IEEE International Symposium on* , vol., no., pp.147,152, 25-29 Aug. 2014
doi: 10.1109/ROMAN.2014.6926245